JOURNAL OF COMPUTATIONAL PHYSICS 96, 428–450 (1991)

Multidomain Spectral Solution of the Euler Gas-Dynamics Equations

DAVID A. KOPRIVA

Department of Mathematics and
Supercomputer Computations Research Institute,
The Florida State University, Tallahassee, Florida 32306

Received December 7, 1989; revised August 14, 1990

We present interface treatments for computing the Euler gas-dynamics equations by a multidomain Chebyshev spectral collocation method. These treatments are suitable for use at the corners of subdomains and for patched or overlapping subdomains. They can be applied to interfaces placed in subsonic, supersonic, or transonic regions of a flow. Computed results indicate that the solutions are spectrally accurate, can be more accurate and more efficient than a single domain calculation, and that reflections of waves at interfaces are not significant. © 1991 Academic Press, Inc.

1. INTRODUCTION

The essential feature of any multidomain spectral method is the procedure used to treat the interfaces between subdomains. For hyperbolic problems, characteristic interface conditions must be applied. A review of early work on such conditions can be found in Canuto *et al.* [1]. More recently, Kopriva [2] described a multidomain method based on a correction-type interface procedure where the solution was computed independently on each subdomain and then corrected afterwards for the propagation of characteristic information. This allowed subdomains to be patched or to overlap, and any subdomain could be refined independently of the others. Quarteroni [3] has also proposed an interface procedure for hyperbolic equations. His procedure differs from that of [2] in that a compatibility condition was solved at an interface.

In one space dimension, the propagation of information through an interface is well defined by the method of characteristics. Consider, for example, a linear hyperbolic system

$$Q_t + AQ_x = 0$$

which, we assume, can be de-coupled to

$$w_t + \Lambda w_x = 0$$

0021-9991/91 $3.00

where $\Lambda = Z^{-1}AZ$ is the real diagonal matrix of eigenvalues of A. The ith component of w is constant along the characteristic curves $x - \Lambda_{ii}t = \text{const}$. At an interface, then, the characteristics with positive slope determine those components of w which are to be computed from information on the left, and the characteristics with negative slope determine those to be computed from the right. For the gas-dynamics equations in one space dimension, the Riemann invariants and the entropy [4] are constant along the characteristics. For subsonic flows, two of these characteristics come from the left and one comes from the right, so the domain of dependence is defined uniquely.

For multidimensional problems, there is usually no unique set of characteristic curves which carry information to a point in space-time. Rather, information propagates along an infinity of bi-characteristic curves which together define the surface of a characteristic cone [5]. To derive treatments for an interface point in multidimensional problems, the authors of [2, 3] effectively chose two particular bi-characteristics. One of these bi-characteristics pointed in the direction of the outward normal to the interface, the other in the direction of the inward normal.

The limitation to the choice of only the two characteristic curves along the normal to an interface is that the normal must vary continuously over the subdomain boundary. This is not the case at the corners of rectangular subdomains. At such points, an ambiguity in the choice of the interface condition arises. In [2], one particular normal was chosen arbitrarily to avoid that ambiguity.

In this paper we describe the solution of both steady and non-steady problems in gas-dynamics by a multidomain Chebyshev spectral method. The method maintains the essential features of [2]: Subdomains can be patched or they can overlap; grid points do not have to match across interfaces so that each subdomain can be refined independently of the others. The new feature is the two-dimensional correction-type interface condition which unambiguously defines subdomain–subdomain and subdomain–physical boundary conditions. The approximation follows historically from the methods developed by Butler [6], Zanetti and Colasurdo [7], and Moretti and Zanetti [8]. Four, rather than two, bi-characteristic curves are chosen to determine the numerical domain of dependence. When the interface normal is continuous, the method reduces to that of Ref. [2].

The method is applied to the steady problems of a subsonic flow in an expanding duct, a transonic flow in a two-dimensional nozzle, and a subsonic flow over a smooth bump. These problems provide examples of subsonic, transonic, and supersonic flows through interfaces and provide examples of several interface topologies. The expanding duct problem has an exact solution and we show that the accuracy is spectral for three grid topologies. In the final problem we consider the acoustic propagation of waves through interfaces and show that reflections at interfaces are not significant.

2. Multidomain Chebyshev Discretization of the Euler Equations

2.1. *The Equations and Interior Point Approximations*

In this paper we consider the solution of the Euler gas-dynamics equations in the non-conservative form

$$\begin{aligned} P_t + \mathbf{q}\cdot\nabla P + \gamma\nabla\cdot\mathbf{q} &= 0 \\ \mathbf{q}_t + \mathbf{q}\cdot\nabla\mathbf{q} + T\nabla P &= 0 \\ s_t + \mathbf{q}\cdot\nabla s &= 0, \end{aligned} \tag{1}$$

where $P=\ln(p)$ is the logarithm of the pressure, $\mathbf{q}=(u, v)$ is the velocity, s is the entropy, and $T=a^2/\gamma$ is the temperature. The sound speed is defined by $a=\sqrt{\gamma}\exp[((\gamma-1)P-s)/2\gamma]$, where $\gamma=1.4$.

The interface treatments which we will derive can also be applied directly to solutions of the conservative form of the equations, though conservation will be lost at the interfaces. No one has yet presented a stable, conservative interface treatment for spectral approximations to hyperbolic equations in conservation form. The reason lies in the fact that only one condition can be specified for each variable at an interface and these conditions are fully specified by the characteristic conditions. The additional restriction of conservation overspecifies the interface conditions.

For each problem, the computational domain is divided into several subdomains denoted by G_{kl} which collectively cover the domain. The subscript refers to grid k on level l. Subdomains on the same level share (patched) boundaries with their neighbors. Subdomains on a higher level overlap those on the lower level. An explanation of how the grids are generated and managed, and how data are interpolated between them, is presented in Ref. [2]. The only difference is that we now use both bilinear mappings and transfinite mappings [9] to define the grids within each subdomain.

On each subdomain, the system (1) takes the form of the quasi-linear system

$$Q_t + AQ_X + BQ_Y = 0, \tag{2}$$

where $Q=[P\ u\ v\ s]^{\mathrm{T}}$. The coefficient matrices are

$$A=\begin{bmatrix} U & \gamma X_x & \gamma X_y & 0 \\ TX_x & U & 0 & 0 \\ TX_y & 0 & U & 0 \\ 0 & 0 & 0 & U \end{bmatrix} \quad \text{and} \quad B=\begin{bmatrix} V & \gamma Y_x & \gamma Y_y & 0 \\ TY_x & V & 0 & 0 \\ TY_y & 0 & V & 0 \\ 0 & 0 & 0 & V \end{bmatrix},$$

where the variables U and V represent the contravariant velocity components $U=uX_x+vX_y$ and $V=uY_x+vY_y$. The spatial part of Eq. (2) is approximated within each subdomain by a standard Chebyshev spectral collocation method [1, 2].

The result of the approximation is a system of ordinary differential equations for the unknowns at each grid point,

$$\mathbf{Q}_t + \mathbf{R}(\mathbf{Q}) = 0, \tag{3}$$

where $\mathbf{R} = [R_\rho \; R_u \; R_v \; R_s]^T$ represents the discretization of the spatial part of (2). Equation (3) is then discretized in time by a two-stage Runge–Kutta procedure

$$\begin{aligned} Q^{(0)} &= Q^n \\ Q^{(1)} &= Q^n + \alpha_1 \Delta t \mathbf{R}(Q^{(0)}) \\ Q^{(2)} &= Q^n + \alpha_2 \Delta t \mathbf{R}(Q^{(1)}) \\ Q^{n+1} &= Q^{(2)}. \end{aligned} \tag{4}$$

To obtain rapid convergence for the steady calculations, we use $\alpha_1 = \alpha_2 = 1$, which corresponds to a forward Euler predictor and backward Euler corrector. The time step is controlled by requiring the Courant number based on the smallest grid spacing to be equal to 0.9. For the (linear) time accurate problem, we use the second order scheme with $\alpha_1 = \frac{1}{2}$ and $\alpha_2 = 1$ and a Courant number of 0.95.

2.2. *Interface Treatment*

For complex problems in gas-dynamics, the interface treatment must be able to define uniquely the solution at various types of interface points such as those shown in Fig. 1. The procedure presented in [2] can handle effectively the subdomain–subdomain and overlap interface points shown in that figure because a unique normal to the interface exists at these points, and information propagates between only two subdomains. At the remaining points shown in Fig. 1, the normal to the interface is not uniquely defined, and information can come from more than two subdomains or physical boundaries.

In order to develop a procedure which unambiguously defines the treatment of

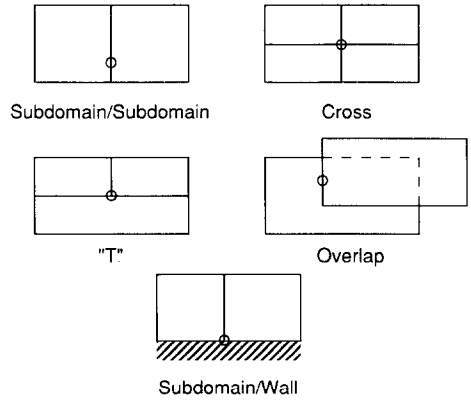

FIG. 1. Examples of subdomain interface points.

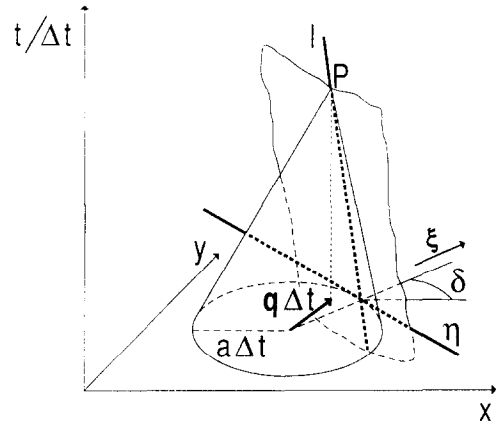

FIG. 2. Domain of dependence of a point, P, in a subsonic flow.

all the interface points in Fig. 1, we recall that for the system (2), information at a particular (x, y, t) comes from an infinity of bi-characteristics which form the surface of a cone [5]. Figure 2 shows the geometry of the situation. Along each bi-characteristic a compatibility can be written which relates derivatives of the unknowns to derivatives tangential to the characteristic cone.

A formal derivation of the compatibility conditions can be found in Butler [6] and these are applicable to general hyperbolic systems of equations. For our purposes, however, the formulation of Zanetti and Colasurdo [7], which is specific to the Euler equations, is most useful. From that paper, we see that the combination of the pressure and momentum equations

$$(P_t + \mathbf{q}\cdot\nabla P + \gamma\nabla\cdot\mathbf{q}) + \frac{\gamma}{a}\left(\mathbf{q}_t + \mathbf{q}\cdot\nabla\mathbf{q} + \frac{a^2}{\gamma}\nabla P\right)\cdot\xi = 0 \tag{5}$$

must hold along each bi-characteristic, where $\xi = \cos(\delta)\hat{x} + \sin(\delta)\hat{y}$ is a normal to the cone. Equation (5) is algebraically equivalent [7] to the equation

$$\frac{DP}{Dt} + \frac{\gamma}{a}\left(\cos(\delta)\frac{Du}{Dt} + \sin(\delta)\frac{Dv}{Dt}\right) = \gamma\left(\sin(\delta)\frac{\partial u}{\partial\eta} - \cos(\delta)\frac{\partial v}{\partial\eta}\right) \tag{6}$$

which relates derivatives along a particular bi-characteristic,

$$\frac{D}{Dt} = \frac{\partial}{\partial t} + (u + a\cos(\delta))\frac{\partial}{\partial x} + (v + a\sin(\delta))\frac{\partial}{\partial y}$$

to derivatives along the tangential direction

$$\frac{\partial}{\partial\eta} = -\sin(\delta)\frac{\partial}{\partial x} + \cos(\delta)\frac{\partial}{\partial y}.$$

The entropy is constant along characteristics and its equation is already in the characteristic form

$$\frac{Ds}{Dt}=\frac{\partial s}{\partial t}+u\frac{\partial s}{\partial x}+v\frac{\partial s}{\partial y}=0. \tag{7}$$

For our purposes, these bi-characteristic curves define the domain of dependence of the solution at an interface point. They are equally useful for defining the domain of dependence at physical boundaries [10].

To actually compute the solutions at an interface, we will derive a correction procedure based on Eq. (5), where the solutions are first computed on the interface by the interior point equations and are later corrected to account for the characteristic waves. Reference [2] proposed the use of such a procedure at subdomain interfaces and argued that it is more efficient than directly solving the compatibility equations (as done in [3]) if, because grid points did not match, one must interpolate data between subdomains. Correction boundary procedures based on characteristics have also been described by Gottlieb *et al.* [11] and Förster [12].

To derive the new interface procedures, we require the computed flow variables at each interface point to satisfy the same compatibility relations, (5), as the true solutions. To accomplish this, we replace the first two equations of (1) by the first two equations of the discretized system, (3), in the compatibility equation, (5). If we call $\mathbf{R}_q \equiv R_u \hat{x} + R_v \hat{y}$, the discrete compatibility condition which must be satisfied at each interface grid point is

$$(P_t + R_p) + \frac{\gamma}{a}(\mathbf{q}_t + \mathbf{R}_q)\cdot\xi = 0. \tag{8}$$

The second speed, a, is a nonlinear function of P and is evaluated at the grid point in question. For convenience, let us now define the new variables $\tilde{P}$ and $\tilde{\mathbf{q}}$ to be the solutions at a boundary or interface point obtained by solving the system (3). That is,

$$\tilde{P}_t = -R_p$$
$$\tilde{\mathbf{q}}_t = -\mathbf{R}_q.$$

With this substitution, Eq. (8) becomes

$$(P_t - \tilde{P}_t) + \frac{\gamma}{a}(\mathbf{q}_t - \tilde{\mathbf{q}}_t)\cdot\xi = 0. \tag{9}$$

Again, Eq. (9) tells how the true computed solution $(P, \mathbf{q})$ and the solution computed by the interior point equations $(\tilde{P}, \tilde{\mathbf{q}})$ must be related along each

bi-characteristic. To obtain the desired correction procedure, we integrate (9) from time level n to $n+1$

$$\int_{t_n}^{t_{n+1}} (P_t - \tilde{P}_t)\, dt + \gamma \xi \cdot \int_{t_n}^{t_{n+1}} \frac{\mathbf{q}_t - \tilde{\mathbf{q}}_t}{a}\, dt = 0. \tag{10}$$

The second integral is approximated by evaluating the sound speed at t_n. Then

$$\begin{aligned}
&(P^{n+1} - \tilde{P}^{n+1}) + \frac{\gamma}{a^n} (\mathbf{q}^{n+1} - \tilde{\mathbf{q}}^{n+1}) \cdot \xi \\
&\quad = (P^n - \tilde{P}^n) + \frac{\gamma}{a^n} (\mathbf{q}^n - \tilde{\mathbf{q}}^n) \cdot \xi \\
&\quad = \left((P^n - \tilde{P}^n) + \frac{\gamma}{a^{n-1}} (\mathbf{q}^n - \tilde{\mathbf{q}}^n) \cdot \xi \right) - \gamma \frac{a^n - a^{n-1}}{a^n a^{n-1}} (\mathbf{q}^n - \tilde{\mathbf{q}}^n).
\end{aligned} \tag{11}$$

The second term of the second line is the product of two factors which are both $O(\Delta t)$. Then to order Δt^2, Eq. (11) yields the compatibility condition at the new time level (leaving off superscripts)

$$(P - \tilde{P}) + \frac{\gamma}{a} (\mathbf{q} - \tilde{\mathbf{q}}) \cdot \xi = 0 \tag{12a}$$

or

$$P + \frac{\gamma}{a} \mathbf{q} \cdot \xi = \tilde{P} + \frac{\gamma}{a} \tilde{\mathbf{q}} \cdot \xi, \tag{12b}$$

provided that the same condition, (12a), is satisfied at the previous time step also. Equation (12b) defines how the generalized Riemann variable $P + (\gamma/a)\mathbf{q} \cdot \xi$ at time level $n+1$ is related to the solution computed from the interior point equations. It is a generalization of the one-dimensional results of Gottlieb *et al.* [11] who required that (as a boundary condition) the true characteristic variable must be equal to the computed one. In this case, however, we have defined an infinity of generalized characteristic variables.

Because the entropy equation, (7), is already in characteristic form, the only correction that is necessary is to set $s = \tilde{s}$, where $\tilde{s}$ is the computed value chosen from the subdomain lying upstream from the interface point.

We remark that the linearization error can be eliminated for the gas-dynamics equations if the flow is homentropic by realizing that

$$aP_t = \frac{2\gamma}{\gamma - 1} a_t. \tag{13}$$

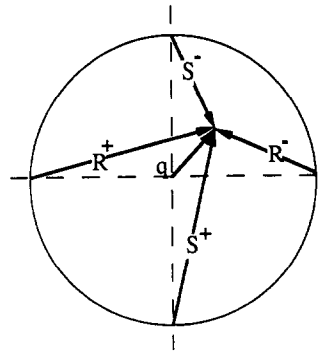

FIG. 3. Projection of the bi-characteristic cone onto the $x-y$ plane showing the choice of four bi-characteristics and the associated Riemann variables.

When (13) is substituted into (9) and integrated in time,

$$\frac{2}{\gamma-1}(a^{n+1}-\tilde{a}^{n+1})+(\mathbf{q}^{n+1}-\tilde{\mathbf{q}}^{n+1})\cdot\boldsymbol{\xi}=0. \tag{14}$$

Equation (14) gives an alternative definition of the compatibility condition (12) which can be used to derive the interface conditions.

Since we are using low order temporal approximations and, in this paper, are primarily interested in the steady state, we are not concerned with the linearization error and have used (12b) rather than (14) in our interface conditions below. For the (linear) time-dependent acoustics problem which we solve, this linearization error does not exist.

We are now in the position to derive the final interface conditions. The procedure described in [2] effectively chooses two of the bi-characteristics, $\boldsymbol{\xi}=\pm\mathbf{N}$, where $\mathbf{N}$ is the normal to the interface, to solve for the pressure and the velocity. To be able to compute all the interface points shown in Fig. 1, including corner points, we follow the procedures of [6–8] and select *four* particular bi-characteristics which lie at positions 90° apart around the characteristic cone. Figure 3 shows an example, for a subsonic flow, of the projection onto the $x-y$ plane of the bi-characteristic cone, the four bi-characteristics and the streamline for the particular choice of $\delta=0$, π, $\pi/2$, $3\pi/2$. From Eq. (12) we have associated with the four bi-characteristics the four Riemann variables:

$$\begin{aligned} R^{\pm} &\equiv P\pm\frac{\gamma}{a}u=\tilde{P}\pm\frac{\gamma}{a}\tilde{u} \\ S^{\pm} &\equiv P\pm\frac{\gamma}{a}v=\tilde{P}\pm\frac{\gamma}{a}\tilde{v}. \end{aligned} \tag{15}$$

The four equations of (15) and the equation $P = \tilde{P}$ form an overdetermined algebraic system for the flow variables. By combining them appropriately we can solve for the three variables P, u, v at any boundary or interface point.

The choice of which Riemann variables are computed from which subdomains or boundaries depends on the origin of the particular bi-characteristic. It is important to recall at this point that a spectral method is global within each subdomain. Thus, the values of each generalized Riemann variable are computed from all points within a subdomain. The choice of the four bi-characteristics, then, merely tells us from which subdomain we will take a particular Riemann variable. One cannot, as in the finite difference methods of Refs. [7, 8], locally modify the stencil to "upwind" the evaluation of a particular Riemann variable.

As examples of how to combine (15) to obtain interface procedures, we now derive conditions for the subdomain–subdomain, wall–interface, and cross points shown in Fig. 1:

(i) *Subdomain–subdomain interface.* Figure 4a shows a schematic of a point at the interface between two subdomains where the flow is subsonic. The subdomain on the right has a finer grid in the vertical direction than the subdomain on the right so the grid lines are not continuous across the interface. It is clear from the figure that the Riemann variables $S^{\pm}$ and R^{+} must be computed from the subdomain on the left while R^{-} must be computed from the right. Since there is no boundary grid point in the right subdomain, R^{-} must be interpolated. (See [2] for the procedure.) The particular choice of bi-characteristics simplifies the computation of the velocity components. To obtain the vertical velocity component, we combine S^{+} and S^{-} to obtain

$$v = \frac{a}{2\gamma}(S_{\mathrm{L}}^{+} - S_{\mathrm{L}}^{-}) = \tilde{v}_{\mathrm{L}}, \tag{16}$$

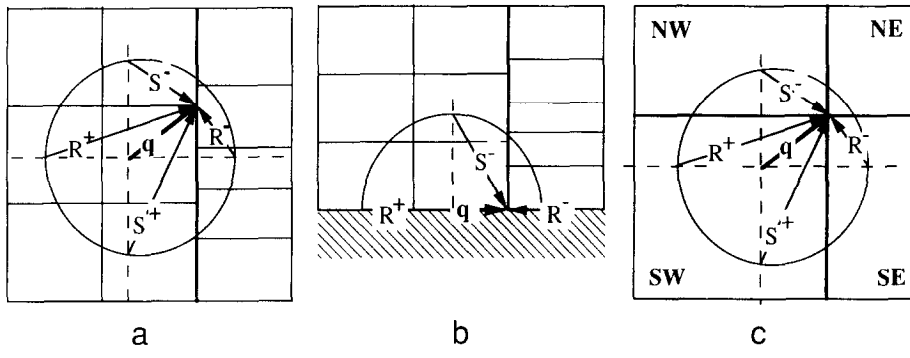

FIG. 4. Domain of dependence of three interface points in a subsonic flow: (a) subdomain–subdomain point; (b) subdomain–wall point; (c) cross point.

where the subscript L refers to the value computed from the interior point scheme in the left subdomain. Thus, the correct value of v at the interface is just the velocity computed in the subdomain on the left. To compute the horizontal velocity component, R^+ and R^- are combined to yield

$$u=\frac{a}{2\gamma}(R_{\mathrm{L}}^{+}-R_{\mathrm{R}}^{-}). \tag{17}$$

These results, (16) and (17), are identical to those one would obtain by the procedure described in [2].

The formula for the pressure is only slightly more complicated. A simple average of the four Riemann variables

$$P=\tfrac{1}{4}(R_{\mathrm{L}}^{+}+R_{\mathrm{R}}^{-}+S_{\mathrm{L}}^{+}+S_{\mathrm{L}}^{-})=\tfrac{1}{4}(3\tilde{P}_{\mathrm{L}}+\tilde{P}_{\mathrm{R}})+\frac{\gamma}{4a}(\tilde{u}_{\mathrm{L}}-\tilde{u}_{\mathrm{R}}) \tag{18}$$

does not give the same correction formula

$$P=\tfrac{1}{2}(\tilde{P}_{\mathrm{L}}+\tilde{P}_{\mathrm{R}})+\frac{\gamma}{2a}(\tilde{u}_{\mathrm{L}}-\tilde{u}_{\mathrm{R}}) \tag{19}$$

that would be correct, since the boundary is smooth, if only two characteristics were chosen. Equation (19) is also the correct formula that should be applied when the vertical velocity vanishes, i.e., when the flow is one-dimensional. The fact that the system of equations which defines P, u, and v is overdetermined, however, gives us the freedom to choose combinations of the Riemann variables which will calculate the pressure in a manner consistent with the one-dimensional problem. Taking a cue from [6, 7], we note that one further solution for the pressure is the value obtained from the interior point calculation, i.e., $P=\tilde{P}$, which is an approximation to the solution computed along the streamline. If we subtract twice this equation from the sum of the four equations, (15),

$$P=\tfrac{1}{2}(R_{\mathrm{L}}^{+}+R_{\mathrm{R}}^{-}+S_{\mathrm{L}}^{+}+S_{\mathrm{L}}^{-}-2\tilde{P}_{\mathrm{L}})=\tfrac{1}{2}(\tilde{P}_{\mathrm{L}}+\tilde{P}_{\mathrm{R}})+\frac{\gamma}{2a}(\tilde{u}_{\mathrm{L}}-\tilde{u}_{\mathrm{R}}). \tag{20}$$

This is now identical to what would be obtained by the procedure described in [2] and is consistent with a one-dimensional flow.

(ii) *Wall–interface boundary.* An example of a case where one has a choice of two normals at an interface point is shown in Fig. 4b, which depicts a point at the intersection of an interface and a wall in a subsonic flow which moves from left to right. The physical boundary condition which must be applied is that the normal velocity component, v, vanishes. From the figure, we see that R^+ and S^- must be

computed from the left while R^- must be computed from the right. The tangential velocity component is computed from $R^{\pm}$,

$$u = \frac{a}{2\gamma}(R_L^+ - R_R^-). \tag{21}$$

To compute the pressure at the interface point, we set $v = 0$ and use the fact that this condition can be viewed as being created by an equivalent S^- coming from below (cf. Moretti [10]). Thus,

$$P = \tfrac{1}{2}(R_L^+ + R_R^- + 2S_L^- - 2\tilde{P}_L) = \tfrac{1}{2}(\tilde{P}_L + \tilde{P}_R) + \frac{\gamma}{2a}(\tilde{u}_L - \tilde{u}_R) - \frac{\gamma}{a}\tilde{v}_L. \tag{22}$$

This formula is not equivalent to what one would obtain if one chose either the vertical or the horizontal normal at the interface point. Neither is it equal to the formula one would obtain by averaging the one-dimensional formulas for each direction, for that average would include a downstream dependence on $\tilde{v}_R$. It is, however, consistent with what one would obtain if the flow were purely one-dimensional in the horizontal direction because in that case, $\tilde{v}_L = 0$. Numerical experience indicates that averaging the two locally one-dimensional formulas is unstable, while Eq. (22) provides a stable procedure.

(iii) *Cross point subdomain intersection.* Figure 4c shows the situation at a cross point. In this case,

$$v = \frac{a}{2\gamma}(S_{SW}^+ - S_{NW}^-) \tag{23}$$

$$u = \frac{a}{2\gamma}(R_{SW}^+ - S_{SE}^-) \tag{24}$$

and

$$P = \tfrac{1}{2}(R_{SW}^+ + R_{SE}^- + S_{SW}^+ + S_{NW}^- - 2\tilde{P}_{SW}). \tag{25}$$

Notice that, in terms of the Riemann variables, the interface conditions Eqs. (23)–(25) are identical in form to Eqs. (17), (18), and (20). In fact, all (internal) interface conditions are governed by the same three equations, when written in terms of the Riemann variables.

If the interfaces or boundaries are not aligned with the $x-y$ axes, it is still possible to use the procedure described above. In such cases one needs only to change the choices of δ. As an example, we consider the wall boundary shown in Fig. 5. The physical boundary condition is that the normal velocity $\mathbf{q} \cdot \mathbf{N} = 0$. The

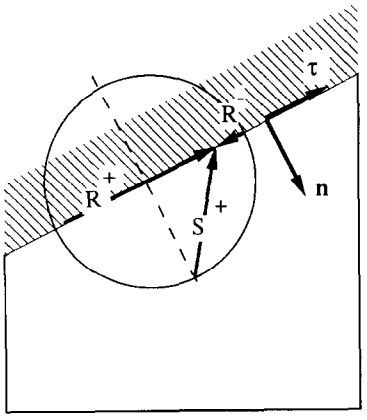

FIG. 5. Choice of bi-characteristics when a boundary is not aligned with the $x-y$ axes.

Riemann variables are computed in the directions tangential and normal to the wall:

$$R^{\pm} = \tilde{P} \pm \frac{\gamma}{a} \tilde{\mathbf{q}} \cdot \boldsymbol{\tau}$$
$$S^{\pm} = \tilde{P} \pm \frac{\gamma}{a} \tilde{\mathbf{q}} \cdot \mathbf{n}. \tag{26}$$

These can be combined to give the tangential velocity and the pressure. The tangential velocity and the boundary condition are sufficient to compute the velocity components u and v. To compute the pressure, we follow the same steps that were used to obtain (22) with these particular Riemann variables.

Actual implementation of the interface and boundary conditions is straightforward. At the end of each time step, the directions of the four bi-characteristics and the streamline are determined from the flow variables for each point on the boundary of a subdomain. These directions, in turn, determine the subdomains from which the Riemann variables are to be computed. Once the Riemann variables are evaluated, the corrected flow variables can be found. The procedure is valid in both subsonic and supersonic flows. It is even applicable if the conservative form of the Euler equations is used. In that case, one would need only to calculate P, u, v, and a from the conservative variables, correct them, and convert back.

Finally, the interface procedures can be extended to three space dimensions by the introduction of two additional Riemann variables

$$G^{\pm} \equiv P \pm \frac{\gamma}{a} w = \tilde{P} \pm \frac{\gamma}{a} \tilde{w}, \tag{27}$$

where $\tilde{w}$ is the computed value of the vertical velocity component. One would then compute w by combining $G^{\pm}$ in the same way that $R^{\pm}$ and $S^{\pm}$ are combined to compute u and v. To compute the pressure, one adds the six Riemann variables and subtracts *four* times $\tilde{P}$ computed along the streamline to give a correction procedure which is consistent with a one- or two-dimensional flow.

3. Numerical Examples

We now consider four numerical examples. The first three are steady flows: Subsonic flow in an expanding duct, the transonic flow in a converging–diverging nozzle and subsonic flow over a bump. The final problem is a linear acoustics example designed to test the effect on the propagation of waves of resolution changes at interfaces.

(1) *Subsonic flow in a diverging duct.* The flow of a steady, irrotational gas from a point source can be solved exactly by a hodograph transformation [4]. In this flow, the streamlines are radial and, for the purposes of this calculation, two of them are chosen as walls of a duct. Finite difference solutions of the subsonic flow case were analyzed in detail by Moretti and Pandolfi [13]. For our example we choose a duct with lower wall $y = 0$ and upper wall $y = x \tan(\pi/6)$ for x between 1 and 1.5. As boundary conditions, we specify that the normal velocity vanish along the upper and lower walls. At the exit, $x = 1.5$, we specify the pressure from the exact solution. At the inflow at $x = 1$, we specify the incoming Riemann variable, R^{+}, from the exact solution, and the angle of the flow by the relation $v = yu$. The solutions were started with an initial gas at rest, i.e., $P = u = v = 0$, and marched in time until steady state was reached.

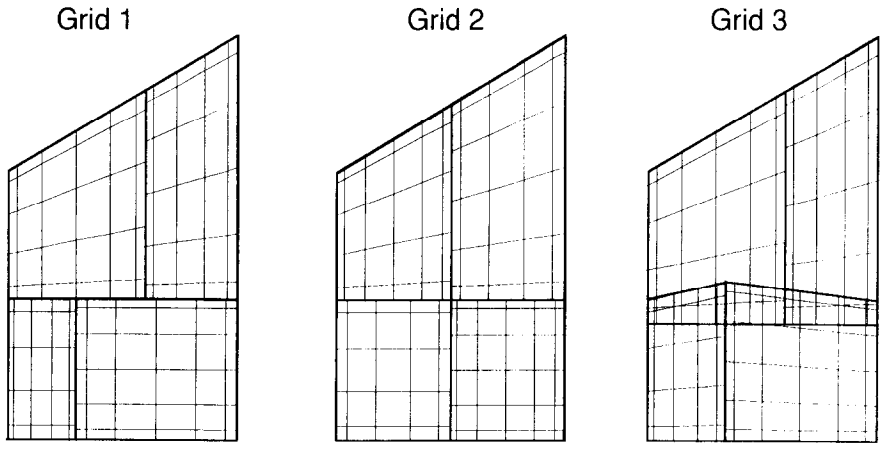

FIG. 6. Three grid topologies for the subsonic flow in a two-dimensional duct.

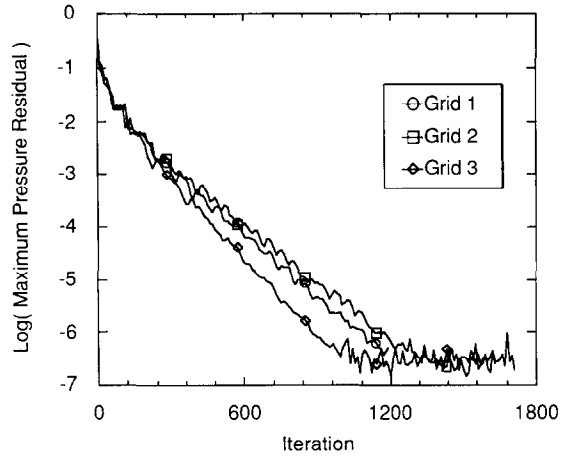

FIG. 7. Residual history for the solutions on the three grids of Fig. 6.

The calculations were performed on the three subdomain topologies shown in Fig. 6. These grids contain all of the interface types shown in Fig. 1 plus others such as inflow–interface or outflow–interface boundary points. In particular, Grid 1 contains two "T" intersections, and Grid 2 contains a single "cross" intersection. Both contain subdomain–wall interfaces. Grid 3 contains "T" intersections and overlapping subdomains, as well as subdomain–wall interfaces.

The solutions on the different grid topologies all converge to steady state. Figure 7 shows the history of the maximum pressure residual for the grids shown in Fig. 6. All three converged to the 32-bit machine accuracy to which the solutions were computed by 1200 time steps. We do not consider the differences in the

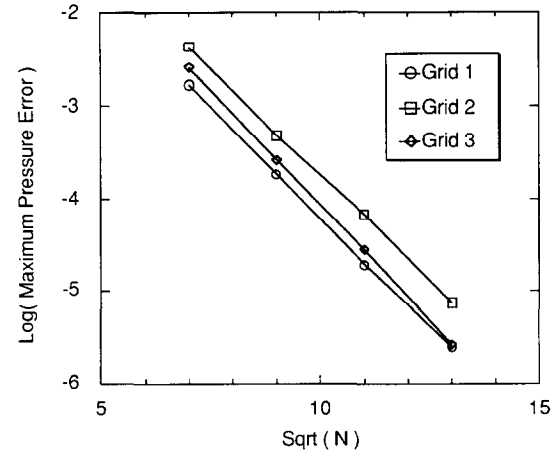

FIG. 8. Maximum error in the pressure for the three grids of Fig. 6 as a function of the total number of grid points.

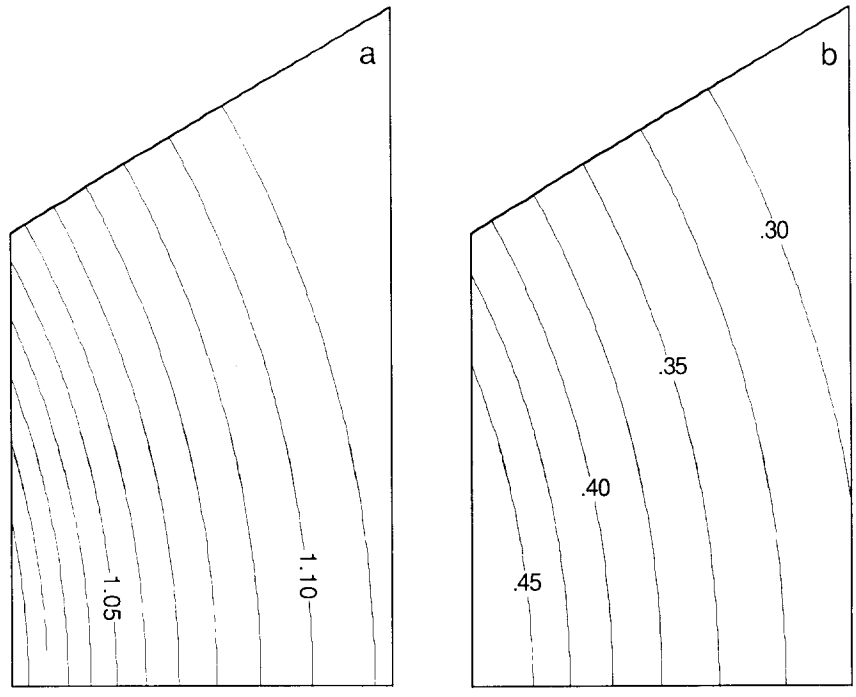

FIG. 9. Solution contours on grid 3 of Fig. 6: (a) pressure; (b) mach number.

convergence rates to be significant. Since the time steps were chosen by a Courant condition based on the smallest grid spacing, Grid 3 had a larger time step than the other two.

Spectral accuracy is observed for this problem. Figure 8, which plots the maximum error in the pressure as a function of the total number of grid points, shows that the error decays exponentially fast on all three grids. Furthermore, the solutions pass smoothly through the interfaces. Figure 9 plots the pressure and Mach number contours for Grid 3 of Fig. 6. For plotting purposes, these and all other contour plots in this paper have been "expanded" by interpolating the results on each subdomain to a fine grid (32 points in each direction) and contouring each subdomain independently. Note that even in the overlap regions the contours pass continuously between subdomains.

(2) *Transonic flow in a two-dimensional converging–diverging nozzle.* The interface procedure described above is valid for subsonic, transonic, and supersonic interfaces. For an example, with all three types, we consider the transonic flow in a two-dimensional converging–diverging nozzle with area variation

$$A(x) = 1 + \cos^2\left(\frac{2\pi x}{2\pi + x}\right)$$

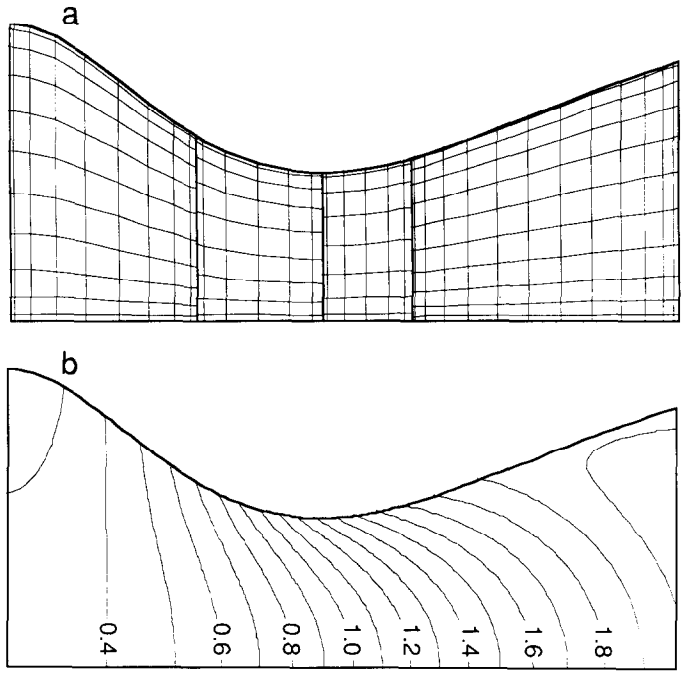

FIG. 10. Grid (a) and Mach contours (b) for steady transonic flow in a two-dimensional nozzle.

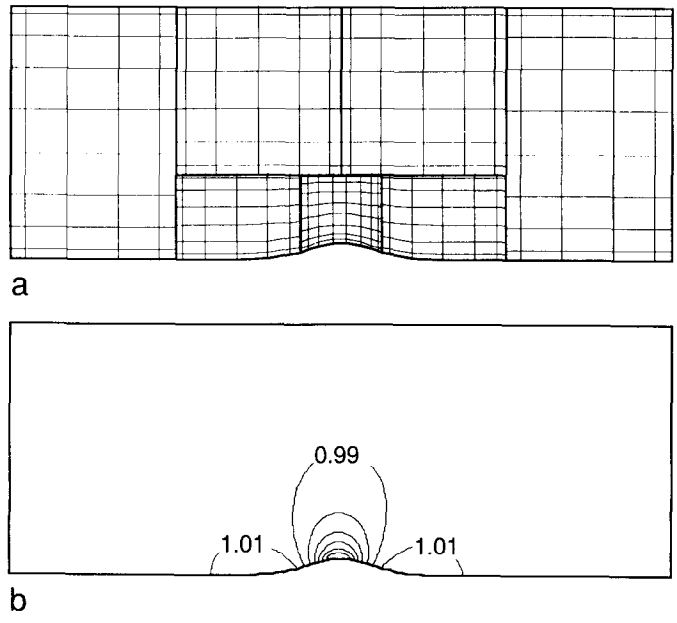

FIG. 11. Grid (a) and pressure (b) contours for a seven domain calculation of subsonic flow over a Gaussian shaped bump.

which has its throat at $x = 2\pi/3$. The nozzle was computed on the interval $0 \leqslant x \leqslant 4.5$. At the inflow at $x = 0$, we specified R^+ from the exact solution of the quasi-one-dimensional approximation and $v = 0$. No boundary condition was specified at the supersonic outflow boundary on the right. The calculation was begun with the solution of the quasi-one-dimensional approximation and marched in time until steady state was reached.

Figure 10 shows the Mach contours and the grid for a calculation where four subdomains were used. The solution was computed for 2000 time steps and was converged to six digits after 1900. Interfaces were chosen so that one would fall in the subsonic portion of the nozzle and one in the supersonic portion. The final interface was placed at the throat so that it would have both subsonic and supersonic points along it. Note that the Mach contours are continuous and smooth across all three interfaces.

(3) *Subsonic flow over a bump.* By careful choice of the subdomains, the multidomain solution of the Euler equations can be both more accurate and more efficient than a single domain calculation. To illustrate this point, we consider calculations made of the external flow over a bump placed in a uniform, subsonic, $M = 0.4$ free stream. The computational domain was specified on the interval $-2 \leqslant x \leqslant 6$ with a bump defined by $y = 0.2 \exp(-(x-2)^2/0.3)$. The upper boundary was placed at $y = 3.5$ which was found to be far enough away to have little effect on the flow near the bottom wall. For the boundary condition on the left, we specified $v = 0$ and the incoming Riemann variable from the free stream, R^+_∞. On the right and top we specified R^-_∞ and S^-_∞, respectively. Free stream initial conditions were used.

Figure 11 presents the grid and pressure contours of a calculation which used seven subdomains and a total of 425 grid points. The subdomains were refined so that the best resolution occurred in the neighborhood of the bump, i.e., where the flow was most disturbed from its free stream values. The solution was computed for 2900 time steps and was converged by roughly 2200. Figure 12 compares the pressure coefficient, defined as $C_p = (p - p_\infty)/(\rho_\infty a^2_\infty)$, for a single domain case and same number of grid points in each direction as the seven domain calculation and it converged by roughly 2900 time steps. The seven domain solution is clearly better than the single domain solution which has oscillations because it could not resolve the variation of the flow near the bump.

In addition to being more accurate, the multidomain calculation is more efficient. In this case, the single domain calculation required a factor of 3.3 more (scalar, 32 bit) cpu time than the seven domain calculation. The reason for the increase in efficiency is twofold (cf. Kopriva [14]). First, since matrix multiplication is used, the work of the derivative evaluations is quadratic in the number of grid points. Thus, it is less expensive to compute the derivatives on the several small (in number of grid points) subdomains than it is on one large subdomain. (We note, also, that round-off errors are significantly reduced by using fewer numbers of grid points.)

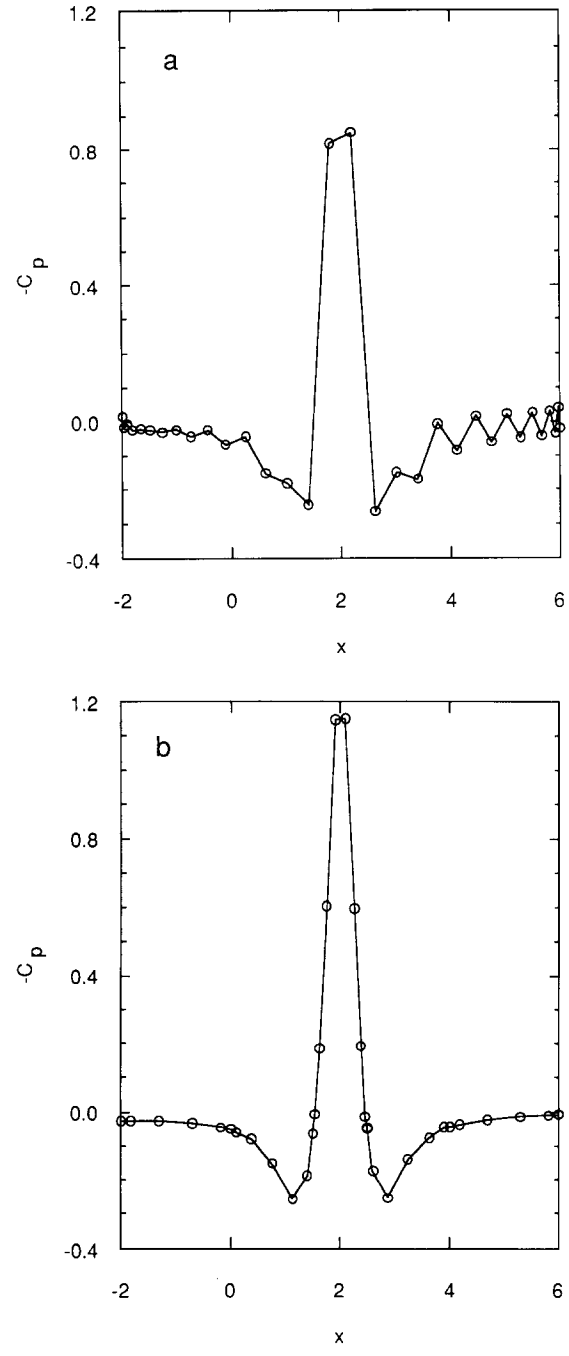

FIG. 12. Pressure coefficient along the bottom boundary of the flow over a bump: (a) single domain calculation; (b) seven domain calculation.

Second, the maximum time step that can be used depends nonlinearly on the order of the Chebyshev expansions in a given subdomain. Thus, it was also possible to use a larger time step on the seven domain calculation. The two calculations converged at roughly the same physical time, but the multidomain calculation required fewer time steps to get there. These two positive factors are balanced by the overhead of interpolating and transferring the data at the subdomain interfaces, which is clearly the lesser effect.

(4) *Acoustic propagation through subdomain interfaces.* Our final example concerns the propagation of waves through subdomain interfaces. It is well known (e.g., [15]) that the large group velocity errors which are characteristic of finite difference methods produce spurious reflections of waves passing through abrupt changes in grid resolution. Though there are no theoretical results regarding the phase or group velocity errors of Chebyshev spectral methods, previous papers [2, 14] have indicated that for a multidomain spectral method, reflections from interfaces are not a serious problem in one space dimension. We show that, with the interface procedure developed above, this conclusion is still valid in two space dimensions.

To derive the equations which govern the propagation of acoustic waves in a constant mean flow, we apply the acoustic approximation

$$\begin{aligned} P &= P_0 + \varepsilon P' \\ u &= u_0 + \varepsilon u' \\ v &= v_0 + \varepsilon v' \end{aligned} \tag{28}$$

to the Euler equations (2). Under this linearization, the coefficient matrix matrices become

$$A = \begin{bmatrix} U_0 & \gamma X_x & \gamma X_y \\ T_0 X_x & U_0 & 0 \\ T_0 X_y & 0 & U_0 \end{bmatrix} \quad \text{and} \quad B = \begin{bmatrix} V_0 & \gamma Y_x & \gamma Y_y \\ T_0 Y_x & V_0 & 0 \\ T_0 Y_y & 0 & V_0 \end{bmatrix}.$$

We specify the initial and boundary conditions so that the exact solution to the problem is a plane Gaussian wave which travels at an angle, θ, to the horizontal,

$$\begin{aligned} p(x, y, t) &= \exp(z) \\ u(x, y, t) &= \frac{\psi}{\sqrt{\gamma}} \exp(z) \\ v(x, y, t) &= \frac{\varphi}{\sqrt{\gamma}} \exp(z), \end{aligned} \tag{29}$$

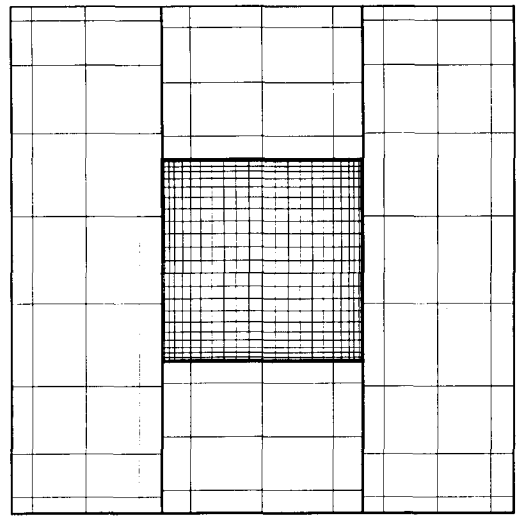

FIG. 13. Grid used for propagation of acoustic waves through interfaces.

where

$$z = \left[x\psi + y\varphi - \sqrt{\gamma}\left(1 + \frac{u_0\psi}{\sqrt{\gamma}} + \frac{v_0\varphi}{\sqrt{\gamma}}\right) t \right]^2 \Big/ \sigma.$$

Here, $\mathbf{k} = (\psi, \varphi) = (\cos(\theta), \sin(\theta))$ is the direction of the wavevector. For our calculations, we set $(u_0, v_0) = (1, 1)$ so that the mean flow was 45° to the horizontal. The parameter $\sigma = 0.05$ was chosen so that the wave packet was just resolved by the coarse grids.

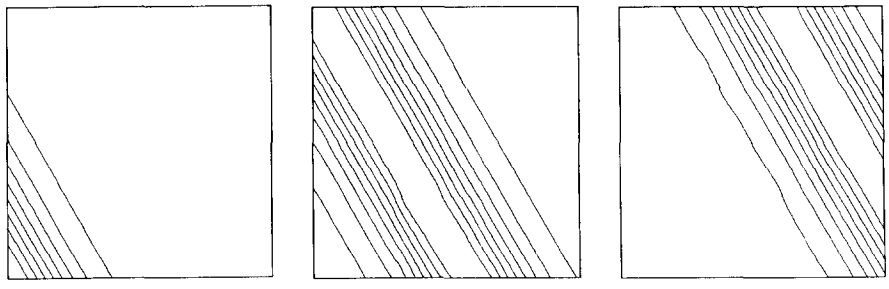

FIG. 14. Pressure contours of acoustic wave with $\theta = \pi/6$ propagating through the grid of Fig. 13 at three times: (a) $t = 0.0$; (b) $t = 0.2$; (c) $t = 0.4$.

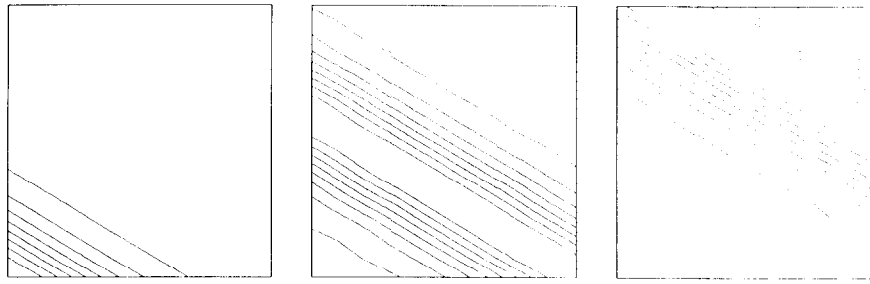

FIG. 15. Pressure contours of acoustic wave with $\theta = \pi/3$ propagating through the grid of Fig. 13 at three times: (a) $t = 0.0$; (b) $t = 0.2$; (c) $t = 0.4$.

The boundary value problem solved on the square domain $(x, y) \in [-1, 1] \times [-1, 1]$ shown in Fig. 13 which has been subdivided into the five subdomains:

$$G_{11} = [-1, -0.3] \times [-1, 1]$$
$$G_{21} = [-0.3, 0.3] \times [-1, -0.3]$$
$$G_{31} = [0.3, 1] \times [-1, 1]$$
$$G_{41} = [-0.3, 0.3] \times [0.3, 1]$$
$$G_{51} = [-0.3, 0.3] \times [-0.3, 0.3].$$

The grid G_{51} used 25 grid points in each direction so that the change in resolution was roughly a factor of five between it and the surrounding subdomains.

We present results for the two values of $\theta = \pi/3$ and $\theta = \pi/6$. Neither the mean flow nor the wavevector were aligned to the grid lines or to the subdomain boundaries. Figure 14 shows the pressure contours at times $t = 0.0$, 0.2, and 0.4 for $\theta = \pi/6$. These times correspond to the initial condition, shortly after the wave crest passes into the fine grid, G_{51}, and shortly after the wave crest leaves the fine grid. The contours represent the range of pressure between 1.1 and 2.5 plotted at an interval of 0.1. Figure 15 shows the results for $\theta = \pi/3$. In neither case is there evidence of significant reflections at the interfaces nor a systematic phase shift between the solutions on the fine and coarse grids. These results suggest that the group velocity errors of the spectral method are very low and that the interface treatment allows waves to pass without reflections even if the waves are not aligned to the interface. We have also computed solutions with overlapping subdomains and the same conclusions can be reached from those results.

4. CONCLUSIONS

We have presented an interface treatment which enables the multidomain spectral method presented in Ref. [2] to solve the Euler gas-dynamics equations.

The treatment differs from that of Ref. [2] in that it uses four bi-characteristics rather than two to determine the domain of dependence at each interface/boundary point. In this way, it allows the unique specification of the interface/boundary points in a smooth two-dimensional flow. Nevertheless, along portions of an interface where the normal is continuous, the technique reduces to that of Ref. [2].

The correction-type scheme presented in Ref. [2] has been retained by the new interface procedures. Though we have not tested it, it should be possible to apply in three space dimensions. The procedure allows the solution to be computed independently on each subdomain and then corrected independently for each interface. Thus, there is significant coarse-grained parallelism to the method. This fact has been exploited in a parallel version which has run on several computer architectures [16].

The method was applied to four flow problems. From the first, we conclude that the method is convergent and spectrally accurate. The second shows that the interfaces can be subsonic, supersonic, or both, and there is no difficulty near a sonic line. The third problem presents a case where the multidomain solution is clearly more accurate and more efficient than the single domain calculation. The final example suggests that reflections at the interfaces are not significant even with a 5:1 refinement of the subdomains and waves which are not aligned to the interfaces.

One issue we have not addressed in this paper is how to deal with shock waves. The characteristic nature of the interface conditions which we have described precludes the passage of captured shocks from one subdomain to another. Since shock capturing methods for spectral methods are still problematical [1], this is not as serious a problem as it would be for a finite difference method. If shocks are present, however, alternatives are available. One is to fit the shock at a boundary of a subdomain [17, 18]. In this way, the solution is not discretized across the discontinuity and the shock motion is calculated explicitly. An alternative would be to place a subdomain which covers the shock region, if the position of the shock is roughly known before the calculation, and use an accurate finite difference shock capturing scheme in that subdomain. The feasibility of this approach is described in [19].

Acknowledgments

This research was supported in part by the National Aeronautics and Space Administration under Grant NAG1-862 and by the U.S. Department of Energy through Contract DE-FC05-85ER250000.

References

1. C. Canuto, M. Y. Hussaini, A. Quarteroni, and T. A. Zang, *Spectral Methods in Fluid Mechanics* (Springer-Verlag, New York, 1987).
2. D. A. Kopriva, *SIAM J. Sci. Statist. Comput.* **10**, 120 (1989).
3. A. Quarteroni, *SIAM J. Sci. Statist. Comp.* **11**, 1029 (1990).

4. R. COURANT AND K. O. FRIEDRICHS, *Supersonic Flow and Shock Waves* (Springer-Verlag, New York, 1976).
5. R. COURANT AND D. HILBERT, *Methods of Mathematical Physics* (Wiley-Interscience, New York, 1962).
6. D. S. BUTLER, *Proc. R. Soc. Ser. A* **255**, 232 (1960).
7. L. ZANNETTI AND G. COLASURDO, *AIAA J.* **19**, 852 (1981).
8. G. MORETTI AND L. ZANNETTI, *AIAA J.* **22**, 758 (1984).
9. W. J. GORDON AND C. A. HALL, *Int. J. Numer. Methods Eng.* **7**, 461 (1973).
10. G. MORETTI, in *Numerical Boundary Condition Procedures*, NASA CP 2201, 1982, p. 73.
11. D. GOTTLIEB, M. GUNZBURGER, AND E. TURKEL, *SIAM J. Numer. Anal.* **19**, 671 (1982).
12. K. FÖRSTER, in *Numerical Boundary Condition Procedures*, NASA CP 2201, 1982, p. 287.
13. G. MORETTI AND M. PANDOLFI, *AIAA J.* **19**, 449 (1981).
14. D. A. KOPRIVA, *Appl. Numer. Math.* **2**, 221 (1986).
15. L. N. TREFETHEN, *SIAM Rev.* **24**, 113 (1982).
16. B. TRAVERSAT, Ph.D. dissertation, The Florida State University, August 1990 (unpublished).
17. D. A. KOPRIVA, in *Computational Acoustics: Algorithms and Applications*, edited by D. Lee *et al.* (Elsevier, Amsterdam, 1988), p. 377.
18. D. A. KOPRIVA AND M. Y. HUSSAINI, in *Domain Decomposition Methods*, edited by T. F. Chan *et al.* (SIAM, Philadelphia, 1989), p. 340.
19. D. A. KOPRIVA, *Appl. Numer. Math.* **6**, 141 (1989/90).